Biochar Activated by Oxygen Plasma for Supercapacitors

Rakesh Gupta[1], Mukul Dubey[1], Parashu Kharel[3], Zhengrong Gu[2]*, Qi Hua Fan[1]*

[1]Department of Electrical Engineering and Computer Science

[2]Department of Agricultural and Biosystems Engineering

[3]Department of Physics

South Dakota State University, Brookings, South Dakota 57007, USA

*Corresponding authors: qihua.fan@sdstate.edu, zhengrong.gu@sdstate.edu

ABSTRACT

Biochar, also known as black carbon, is a byproduct of biomass pyrolysis. As a low-cost, environmental-friendly material, biochar has the potential to replace more expensive synthesized carbon nanomaterials (e.g. carbon nanotubes) for use in future supercapacitors. To achieve high capacitance, biochar requires proper activation. A conventional approach involves mixing biochar with a strong base and baking at a high temperature. However, this process is time consuming and energy inefficient (requiring temperatures >900°C). This work demonstrates a low-temperature (<150°C) plasma treatment that efficiently activates a yellow pine biochar. Particularly, the effects of oxygen plasma on the biochar microstructure and supercapacitor characteristics are studied. Significant enhancement of the capacitance is achieved: 171.4 F g^{-1} for a 5-minute oxygen plasma activation, in comparison to 99.5 F g^{-1} for a conventional chemical activation and 60.4 F g^{-1} for untreated biochar. This enhancement of the charge storage capacity is attributed to the creation of a broad distribution in pore size and a larger surface area. The plasma activation mechanisms in terms of the evolution of the biochar surface and microstructure are further discussed.

Keywords: supercapacitors, biochar, plasma, activation

1. INTRODUCTION

Energy storage is a critical component of the infrastructure for sustainable energy. Among energy storage options, the supercapacitor plays an irreplaceable role due to its large capacity, fast charge/discharge, and stability [1, 2]. Supercapacitors have seen increased application in electrical automobiles, electrical grids, uninterruptible power supplies, and power tools. To a great extent, the performance of supercapacitors depends on the electrode material and structure. Carbon materials are suitable for electrodes because of their good electrical conductivity, electrochemical stability, and natural abundance. State-of-the-art supercapacitors use chemically synthesized carbon nanomaterials (e.g. carbon nanotubes and graphene), which are expensive and necessitate toxic chemicals for synthesis [3-8]. Active carbons (e.g. YP-50) currently used by industries generally yield unsatisfactory specific capacitance (100 - 150 F g^{-1}). These issues have together driven the search for alternative low-cost and environmental-friendly electrode materials.

Biochar is a carbon-rich material produced through pyrolysis of biomass, such as wood, manure, and crop residues [9]. Biochar has demonstrated promising potential in the field of supercapacitors [10-13]. Among a variety of tested materials, biochar samples derived from a woody mass showed surface areas of ~1000 m^2 $g^{-1}$and capacities of 167 F g^{-1} [14]. Hierarchical carbon with a high specific surface area of approximately 3000 m^2 $g^{-1}$was prepared from distiller-dried grains with solubles (DDGS), and yielded a specific capacitance of 260 F g^{-1}[15]. Even more recently, activated carbon prepared from rice hulls led to a specific capacitance of about 368 F g^{-1} [16] – comparable to that of synthesized carbon nanomaterials [6, 7].

A vital step in using biochar for supercapacitors is the activation of the material, which creates porous nanostructures over a large surface area with optimal pore-size distribution. This

activation currently requires hours of high-temperature treatment (~960°C) in an inert atmosphere using a strong base (KOH) mixed with biochar powder, followed by chemical washing and prolonged drying [13, 14]. This energy-intensive and time-consuming process has become a significant barrier to achieving cost-effective biochar supercapacitors.

This work aims to establish a plasma treatment that efficiently activates biochar for use in supercapacitors. In order to attain highly reactive plasma and sufficient plasma density, oxygen gas was used and excited by radio frequency through a dielectric barrier discharge. This idea was founded on two facts: (1) a dielectric barrier discharge was proven effective in the semiconductor dry etching process, producing negligible contamination; and (2) oxygen plasma was highly reactive to glassy carbon, an element always found in biochar derived from biomass pyrolysis. In this study, yellow pine biochar was selected to demonstrate the effectiveness of oxygen plasma in creating porous morphology. Yellow pine biochar has been previously studied using conventional chemical activation, and the study results were consistent among the reports of different groups. This stable material performance provided a reliable comparison between plasma activation and conventional chemical activation.

Few previous works have mentioned the functionalization of the surface of active carbon materials using plasma; this treatment led to limited improvement in specific capacitance (e.g. 82 to 92 F g^{-1}) [17, 18]. Specifically, there were no reports on using plasma to activate biochar. Therefore, the first part of this work focused on studying the evolution of the microstructure and porosity of yellow pine biochar following oxygen plasma treatment. The second part studied the electrochemical characteristics of supercapacitors fabricated with yellow pine biochar, comparing biochar activated by a conventional chemical process and by oxygen plasma. The

results confirmed that oxygen plasma was very effective in activating yellow pine biochar, as seen in the substantial increase in specific capacitance.

2. EXPERIMENT

Biochar generated from pyrolysis of yellow pine was first ground for 30 minutes using a ball-milling machine. The biochar powder was then activated using either oxygen plasma or a conventional chemical process. The plasma activation was performed using a dielectric barrier discharge, illustrated in Figure 1. The excitation radio frequency (RF) and power were set at 13.56 MHz and 50 W respectively. The flow rate of the reactive gas was controlled using a needle valve that maintained a discharge pressure of ~2 Torr. The treatment time was 5 minutes if not otherwise indicated. The temperature of the sample holder gradually increased with time, stabilizing at just below 150°C. For the chemical activation, the biochar powder was mixed with a NaOH solution (the ratio between NaOH and biochar was 2:1) in a N_2 atmosphere, and dried in a conventional oven at 105°C for 48 hrs. The dried mixture was then heated at 400°C for 6 hrs in the N_2 atmosphere of a muffle furnace (flow rate of 500 ml min^{-1}) to remove water. Activation was then carried out at 950°C for 3 hrs. The activated sample was cooled within the furnace (still in a N_2 atmosphere). After cooling down to room temperature (around 9 hrs), the activated biochar was washed with 0.1 mol L^{-1} HCl and deionized water to reach a pH of 7, and then dried at 105°C for 12 hours in a vacuum.

Fig. 1

The supercapacitor electrodes were prepared using nickel foam (EQ-bcnf-80um from MTI Corp.) and biochar slurry. It was cut into a circular shape with a diameter of 1 cm. The biochar slurry was prepared using treated/untreated biochar mixed with Polytetrafluoroethylene (PTFE), known as a binder, with a mass ratio of 8.5:1.5 for biochar and PTFE respectively. To

form the electrode, the biochar slurry was pressed onto the nickel foam for ~5 minutes using a 1 ton force. The active electrode mass loaded on the nickel foam was of 15 mg per cm^2 consistency, and the resultant total thickness of an electrode was about 310 μm. A layer of biochar, about 230 μm thick, was deposited on top of the compressed nickel foam (~80 μm), the voids of which were filled with biochar. The electrolyte used was 6 mol L^{-1} KOH, which was dissolved into the biochar electrodes. A microporous separator (3501, Celgard) was set between the electrodes. These components were sealed in a CR2032 coin cell case at room temperature.

The composition, structure, and porosity of the biochar were characterized using a variety of analytical methods. Isotherm adsorption of N_2 at 77 K was carried out using an ASAP 2010 Micropore Analyzer. The specific surface area was calculated using the Brunauer-Emmett-Teller (BET) equation. The pore size distribution was determined using Barrett-Joyner-Halenda (BJH) analysis. The structure of biochar was characterized using Horiba Raman spectroscopy at room temperature, with an excitation wavelength of 532 nm from a diode pumped solid-state laser. The surface morphology was characterized using a Hitachi S3400 Scanning Electron Microscope (SEM) and a FEITecnai Spirit G^2 Twin Transmission Electron Microscope (TEM). The elemental analysis was completed using energy dispersive X-Ray spectroscopy (EDX) attached to the SEM system.

Cyclic voltammetry measurement was performed using an Ametek VERSASTAT-450 Potentiostat. The scan rate was20 mVs^{-1}, if not otherwise stated. The cyclic potential sweep was set with an initial and final voltage of -1.0 V and a vertex voltage of 1.0 V. The impedance of the fabricated supercapacitors was measured using impedance spectroscopy, specifically the VERSASTAT-450, with a frequency range of 0.1 Hz to 100 KHz and a potential amplitude of 10 mV. The specific capacitance was calculated from galvanostatic discharge characteristics and

expressed in Farads per gram of active biochar deposited on the electrode. The calculation equation is given below:

$$C = \frac{2I\Delta t}{m\Delta v}$$

I is the charge or discharge current density, Δt is the charge or discharge time, m is electrode mass, and Δv is the total change in voltage.

3. RESULT AND DISCUSSION

3.1. Microstructure and Composition of Biochar

Figure 2 shows SEM images of untreated, plasma activated, and chemically activated biochar. The biochar was grounded for 30 minutes. Afterwards, the biochar contained a mixture of small and large particles (Fig. 2a). Following the plasma activation, the biochar surface became porous, and few large-size particles remained visible (Fig. 2b). These results implied that the plasma selectively etched off certain phases in the biochar. Contrary to the plasma activation, the chemical activation broke down large particles into smaller ones, and eliminated extremely fine particles. The oxygen plasma etching was a rapid process. The yield of biochar depended on the plasma treatment time. After 5-minutes of plasma activation at 50 W RF excitation power, comparing the weight before and after the plasma treatment, the biochar yield was about 80%. As shown in section 3.3, the 5-minute plasma activation yielded a higher specific capacitance than that obtained through a shorter (<2 minutes) or longer (>10 minutes) treatment.

Fig. 2

Further analysis was performed to understand the effects of plasma and chemical activations on the biochar composition and microstructure. Table 1 summarizes the EDX results of the biochar composition before and after activation. For the untreated biochar, Kα lines of carbon and oxygen were very pronounced. Typical ash components, like calcium, silicon, and

magnesium, were also detected, totaling 12.53 wt%. Noticeable variations in the amount of impurity elements (calcium, silicon, and magnesium) present in the plasma activated biochar indicated that these elements most likely arose from random contamination. The oxygen content increased after the plasma treatment, which greatly modified the biochar surface bonds. The chemical activation appeared efficient in removing the impurities, and also led to an increase in the incorporation of oxygen. The chemical bonds between the oxygen and the biochar require further confirmation.

Table 1. Element composition from EDX analysis of different biochar powders.

Element.	Line	Concentration (wt%)		
		Untreated	Plasma activated	Chemically activated
C	Kα	77.61	79.25	84.85
O	Kα	9.86	15.69	12.86
Mg	Kα	2.62	1.62	1.20
Si	Kα	2.35	0.00	0.45
Ca	Kα	7.56	3.44	0.64
Total		100.00	100.00	100.00

Figure 3 shows the Raman spectra of untreated, plasma activated, and chemically activated biochar. The characteristic peak around 1530-1610 cm^{-1} (G-band) corresponded to individual graphite dominated by sp^2 bonds, while the peak around 1320-1370 cm^{-1} (D-band) indicated a disordered and imperfect structure [19]. An increase in I_D/I_G reflected a higher proportion of sp^3 carbon [20, 21]. For the chemically activated biochar, the ratio of I_D/I_G decreased slightly from 0.95 (untreated biochar) to 0.82, indicating a weak selective chemical etching. On the other hand, the signal intensity decreased significantly. A possible explanation, as will be shown later, was that the chemical activation created a highly porous structure, which led to the trapping and/or scattering of the incident laser and Raman signal. For the plasma

activated biochar, in addition to a decrease in the signal intensity (again due to a porous structure), the I_D/I_G ratio increased by more than two times compared to the untreated biochar. This result implied that the oxygen plasma etched sp^2 carbon faster than sp^3 carbon. It is worth noting that the raw Raman signals from the plasma activated and chemically activated biochar samples were one order of magnitude lower than that from the untreated biochar. This low signal intensity was accompanied by noise and background. Therefore, the raw data was processed with Origin software to remove the noise and background for meaningful comparison. The Origin process included curve fitting, linear baseline, and a free constraint calculation of all parameters (including the peak position, height, width, mixing percentage for each peak, and slope and intersection for baseline). What shown in Figure 3 are the fitted curves. TEM images (Figure 4) clearly showed that the plasma activation resulted in the appearance of nano-fibers, which were likely dominated with sp^3 bonds. Note that the TEM images were taken from the edge of the biochar – the thinnest region – because it allowed the most effective imaging. The nano-fiber structure was consistently found all over the plasma treated biochar. For the chemically activated biochar, TEM images revealed a microporous structure (Fig. 4c) in which no nano-fibers were observed.

Fig. 3

Fig. 4

3.2. Porous Morphology of Biochar

Efficiently creating porous morphology in biochar is a desired effect of the activation. A large surface area combined with the proper distribution of pore sizes (micropore, mesopore, and macropore) is the key to achieving high specific capacitance. Isotherm adsorption tests yielded varying cumulative pore volume vs. pore diameter figures for untreated, plasma activated, and

chemically activated biochar, as shown in Figure 5. The untreated biochar had fewer pores in the full test range of 0 – 600 Å pore size. Therefore, it had the lowest cumulative pore volume. Chemical activation created uniform pores with relatively small sizes below 50 Å and the average pore size was 21.6 Å. It appeared that the chemical activation actually removed large pores that existed in the original biochar. The plasma activation created various pores with sizes ranging from micropores (<20 Å) to macropores (>500 Å). The plasma activated biochar included significantly more mesopores compared with chemically activated biochar. In other words, plasma activation created a wider distribution in pore size. As will be discussed later, this pore size distribution seemed to favor ion transportation, leading to lower impedance and higher specific capacitance. It should be noted that a small number of random macropores also existed in the untreated and chemically treated biochar. Hence, cumulative pore volume was used in Fig. 5 to more easily compare the pore distribution over the examined range of pore sizes.

Fig. 5

A detailed BET analysis of the specific area, pore volume, and average pore size is summarized in Table 2. Two important features were observed: (1) The chemical activation led to a larger surface area, but also a smaller pore volume than that of plasma activation; and (2) the average pore size created by chemical activation was much smaller than that created by the plasma. As will be shown in the next section, the pore volume and pore size had a strong impact on the performance of supercapacitors.

Table 2. Comparison of BET surface area and pore morphology of yellow pine biochar.

Treatment	BET Surface Area ($m^2\ g^{-1}$)	Pore Volume ($cm^3\ g^{-1}$)	Average Pore Size (nm)
Untreated	440	0.455	4.8
Plasma activated	654	0.936	4.9
Chemically activated	1144	0.550	2.3

3.3. Electrochemical Characteristics of Biochar Supercapacitors

Figure 6 shows the cyclic voltammetry (CV) curves of supercapacitors fabricated using untreated, oxygen plasma activated, and chemically activated biochar. The specific capacitance was calculated to be 60.4 F g^{-1}, 171.4 F g^{-1}, and 99.5 F g^{-1} for the untreated, plasma activated, and chemically activated biochar, respectively. The specific capacitance of 171.4 F g^{-1} was the highest capacitance achieved for supercapacitors made from yellow pine biochar. The CV curve of the untreated biochar appeared elliptical, while the curves representative of plasma and chemical activation formed more rectangular shapes that were characteristic of an ideal electric double layer capacitor [13, 22]. Therefore, the activation processes not only created a large surface area and pore volume, but also promoted surface energy and chemical structures that favored ion transport, forming the double layer. Note that in the CV measurement the polarity was inverted to confirm the symmetry of the I-V characteristics.

Fig. 6

The large surface area created by the chemical activation did not result in high capacitance as expected. This confirmed that the specific capacitance also depended on the pore size and the size distribution [23-27]. As seen in the previous section, the oxygen plasma was capable of creating various pore sizes that would allow easy access for the electrolyte ions to the porous surface, leading to a higher capacitance than the chemically activated biochar. It is worthy to note that the specific capacitance values presented here were derived from a real two-electrode system, not from a half-cell or single electrode. This is important, as a substantial amount of data in past literatures were gathered from a three-electrode system, which overestimated the specific capacitance [24, 28, 29].

Figure 7 shows the electrochemical impedance spectroscopy (EIS) plots of untreated, plasma activated, and chemically activated biochar supercapacitors. The measured frequency range was from 0.1 Hz to 10 KHz, and the supplied voltage was 10 mV. The estimated resistance values, Re(Z), of the oxygen plasma activated, chemically activated, and untreated biochar supercapacitors were 3.3 Ω, 14.5 Ω, and 8.2 Ω respectively. The low resistance resulting from the plasma activation was, to a great extent, attributed to ions having easy access to micropores and mesopores, as discussed before. It was also noted that the chemical activation led to increased resistance. Further studies are needed to clarify whether or not this is due to the surface chemical structures. It should be noted that the EIS-measured impedance included contributions from both the biochar-based electrodes and the electrolyte. The supercapacitor fabrication process was kept constant; only the biochar activation differed between trials. Therefore, the measured Re(Z) values reflected the effects of only the biochar activation on the material properties and morphologies.

Fig. 7

Figure 8 shows the specific capacitance vs. number of charge/discharge cycles for untreated, oxygen plasma activated, and chemically activated biochar supercapacitors. The current density was 160 mA g^{-1}. The specific capacitance did not change even after 1000 cycles. Although more charge/discharge cycles are still under study, this initial test provided evidence of the stability of plasma activated biochar supercarpacitors.

Fig. 8

Oxygen plasma activation of yellow pine biochar was also performed for different amounts of time: 2, 5, 10, and 30 minutes. The specific capacitance was the highest following a 5 min. treatment, as illustrated in Figure 9. One possible reason for this capacitance variation was

that short plasma activation could not create enough porous morphology, while longer treatments could lead to deeper small pores and the removal of large surface pores. Note that the 5-minute plasma activation was not necessarily the best time condition. It did indicate that there exists an optimal combination of pore size distribution and surface area. However, further systematic studies are needed to clarify the effects of the morphologies created by different plasmas (e.g. H_2, O_2, and N_2) under various conditions (e.g. time, plasma power, and gas pressure) on the characteristics of supercapacitors. Furthermore, although the resistance varied between plasma treatments, the changes were of small increments (1 – 3.3 Ω). Compared with the 8.2 Ω untreated biochar, the plasma activation greatly reduced resistance.

Fig. 9

4. CONCLUSIONS

This first report of plasma activation of biochar demonstrated that oxygen plasma efficiently created porous structures that combined micropores, mesopores, and macropores. While chemical activation created uniformly sized micropores, oxygen plasma activated yellow pine biochar yielded much higher specific capacitance (e.g. 171.4 F g^{-1}) than chemically activated biochar (99.5 F g^{-1}) and untreated biochar (60.4 F g^{-1}). Plasma activation was an efficient (5 min.), non-toxic, and energy-saving approach compared with the conventional chemical activation (~950°C and several hours). This study also showed that a large surface area needed to be combined with a proper pore-size distribution to achieve high specific capacitance. Further research topics include elucidating the surface chemical structures of plasma activated biochar and quantifying the optimal pore size distribution.

5. ACKNOWLEDGEMENTS

This work was supported by the DOE Sun Grant Initiative, North Central Sun Grant Center (DE-FG36-08GO88073), and National Science Foundation (IIP-1248970). Part of this research was based upon work supported by the National Science Foundation/EPSCoR Grant Number 0903804 and the State of South Dakota. Any opinions, findings, and conclusions or recommendations expressed in this material are those of the authors and do not necessarily reflect the views of the National Science Foundation.

REFERENCES

[1] M. Winter and R. Brodd, "What are Batteries, Fuel Cells, and Supercapacitors?", *J. Chem. Rev.*104 (2004), 4245.

[2] M. Vangari, T. Pryor, and L. Jiang, "Supercapacitors: Review of Materials and Fabrication Methods", *J. Energy Engineering* 139 (2012), 72.

[3] E. Frackowiak, K. Metenier, V. Bertagna, and F. Beguin, "Supercapacitor Electrodes from Multiwalled Carbon Nanotubes", *Appl. Phys. Lett.* 77 (2000), 2421.

[4] E. Frackowiak and F. Beguin, "Electrochemical Storage of Energy in Carbon Nanotubes and Nanostructured Carbons", *Carbon* 40 (2002), 1775.

[5] Y.-T. Kim, Y. Ito, K. Tadai, T. Mitani, U.-S. Kim, and H.-S. Kim, "Drastic Change of Electric Double Layer Capacitance by Surface Functionalization of Carbon Nanotubes", *Appl. Phys. Lett.* 87 (2005), 234106.

[6] H. Pan, J. Li, and Y. P. Feng, "Carbon Nanotubes for Supercapacitor", *Nanoscale Research Lett.* 5 (2010), 654.

[7] Y. W. Zhu, S. Murali, M. D. Stoller, K. J. Ganesh, W. W. Cai, R. S. Ruoff, "Carbon-Based Supercapacitors Produced by Activation of Graphene", *Science* 332 (2011), 1537.

[8] Y. Jiang, P. Wang, X. Zhang, Y. Yanmg, A. Kozinda, L. Lin, "Uniformly Embedded Metal Oxide Nanoparticles in Vertically Aligned Carbon Nanotube Forests as Pseudocapacitor Electrodes for Enhanced Energy Storage", *NanoLett.* 13 (2013), 3524.

[9] J. J. Manyà, "Pyrolysis for Biochar Purposes: a Review to Establish Current Knowledge Gaps and Research Needs", *Environmental Science & Technology* 46 (2012), 7939.

[10] T. Funabashi, J. Mizuno, M. Sato, M. Kitajima, M. Matsuura, and S. Shoji, “Film of Lignocellulosic Carbon Material for Self-supporting Electrodes in Electric Doublelayer Capacitors”, *Appl. Phys. Lett.Mater.* 1 (2013), 032104.

[11] X. He, P. Ling, J. Qiu, M. Yu, X. Zhang, C. Yu, and M. Zheng, “Efficient Preparation of Biomass-based Mesoporous Carbons for Supercapacitors with Both High Energy Density and High Power Density”, *J. Power Sources* 240 (2013), 109.

[12] Q. Wang, Q. Cao, X. Wang, B. Jing, H. Kuang, L. Zhou, “A high-capacity carbon prepared from renewable chicken feather biopolymer for supercapacitors”, *J. Power Sources* 225 (2013), 101.

[13] H. Jin, X. Wang, Z. Gu, J. Polin, “Carbon Materials from High Ash Bio-char for Supercapacitor and Improvement of Capacitance with HNO3 Surface Oxidation”, *J. Power Sources* 236 (2013), 285–292.

[14] J. Jiang, L. Zhang, X. Wang, N. Holm, K. Rajagopalan, F. Chen, S. Ma, “Highly Ordered Macroporous Woody Biochar with Ultra-high Carbon Content as Supercapacitor Electrodes”, *ElectrochimicaActa* 113 (2013), 481.

[15] H. Jin, X. Wang, and Z. Gu, “Hierarchical Carbon Materials from High Ash Bio-char of Distiller's Dried Grain with Solubles for Supercapacitor”, *Materials Focus* 12 (2012), 21.

[16] H. Chen, H. Wang, L. Yang, Y. Xiao, M. Zheng, Y. Liu, H. Fu, “High Specific Surface Area Rice Hull Based Porous Carbon Prepared for EDLCs”, *Int. J. Electrochem. Sci.* 7 (2012), 4889.

[17] S. Hussain, R. Amade, E. Jover, and E. Bertran, “Nitrogen Plasma Functionalization of Carbon Nanotubes for Supercapacitor Applications”, *J. Mater.Sci.* 48 (2013), 7620.

[18] G. Lota, J. Tyczkowski, R. Kapica, K. Lota, E. Frackowiak, "Carbon Materials Modified by Plasma Treatment as Electrodes for Supercapacitors", *J. Power Sources* 195 (2010), 7535.

[19] O. Paris, C. Zollfrank, and G. A. Zickler, "Decomposition and carbonisation of wood biopolymers—a microstructural study of softwood pyrolysis", *Carbon* 43 (2005), 53.

[20] K. G. Ray III and R. L. McCreery, "Characterization of the surface carbonyl and hydroxyl coverage on glassy carbon electrodes using Raman spectroscopy", *J. Electroanalytical Chemistry* 469 (1999), 150.

[21] Y. Wang, D. C. Alsmeyer, and R. L. McCreery, "Raman spectroscopy of carbon materials: structural basis of observed spectra", *Chemistry of Materials* 2 (1990), 557.

[22] A. Pandolfo and A. Hollenkamp, "Carbon properties and their role in supercapacitors", *J. Power Sources* 157 (2006), 11.

[23] E. Frackowiak and F. Beguin, "Carbon materials for the electrochemical storage of energy in capacitors", *Carbon* 39 (2001), 937.

[24] D. Qu and H. Shi, "Studies of activated carbons used in double-layer capacitors", *J. Power Sources* 74 (1998), 99.

[25] J. Gamby, P. Taberna, P. Simon, J. Fauvarque, and M. Chesneau, "Studies and characterisations of various activated carbons used for carbon/carbon supercapacitors", *J. Power Sources* 101 (2001), 109.

[26] H. Shi, "Activated carbons and double layer capacitance", *ElectrochimicaActa* 41 (1999), 1633.

[27] H. Pan, C. K. Poh, Y. P. Feng, and J. Lin, "Supercapacitor electrodes from tubes-in-tube carbon nanostructures", *Chemistry of Materials* 19 (2007), 6120.

[28] S. Mayer, R. Pekala, and J. Kaschmitter, “The aerocapacitor: An electrochemical double-layer energy-storage device”, *J. Electrochemical Society* 140 (1993), 446.

[29] E. Raymundo-Pinero, V. Khomenko, E. Frackowiak, and F. Beguin, "Performance of manganese oxide/CNTs composites as electrode materials for electrochemical capacitors," *J. Electrochemical Society* 152 (2005), A229.

List of Figure Captions

Figure 1.The dielectric barrier discharge excited by RF power (creating plasma in a vacuum chamber). The electron – gas interactions include ionization, excitation, and elastic scattering. An example of a reaction between the electrons and gas is an electron colliding with an oxygen atom, creating an oxygen ion and two electrons. The electron – gas interactions generate a large number of reactive species, such as excited oxygen atoms (O*) and oxygen ions (O^+). In this work, a 2" diameter quartz tube was used as the vacuum chamber.

Figure 2. SEM images of (a) untreated, (b) plasma activated, and (c) chemically activated biochar.

Figure 3. Raman spectra of untreated, plasma activated, and chemically activated biochar.

Figure 4.TEM images of (a) untreated, (b) plasma activated, and (c) chemically activated biochar.

Figure 5. Cumulative pore volume vs. pore diameter for untreated, plasma activated, and chemically activated biochar.

Figure 6. CV curves of supercapacitors fabricated from untreated, oxygen plasma activated, and chemically activated biochar. The electrolyte was 6 mol L^{-1} KOH.

Figure 7. EIS curves of untreated, oxygen plasma activated, and chemically activated biochar supercapacitors. The measurement frequency range was 0.1 to 10 KHz and the voltage was 10 mV.

Figure 8. Specific capacitance vs. number of charge/discharge cycles for untreated, oxygen plasma activated, and chemically activated biochar supercapacitors.

Figure 9. Effects of plasma treatment time on the specific capacitance and resistance of the biochar supercapacitors.

List of Table Captions

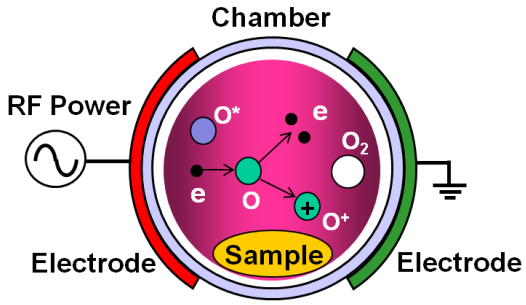

Fig. 1. Dielectric barrier discharge excited by RF power to create plasma in a vacuum chamber. The electron – gas interactions include ionization, excitation, and elastic scattering. An example of a reaction between the electrons and gas is one electron colliding with an oxygen atom, creating one oxygen ion and two electrons. The electron – gas interactions generate a large number of reactive species, such as excited oxygen atoms (O*) and oxygen ions (O^+). In this work, a 2" diameter quartz tube was used as the vacuum chamber.

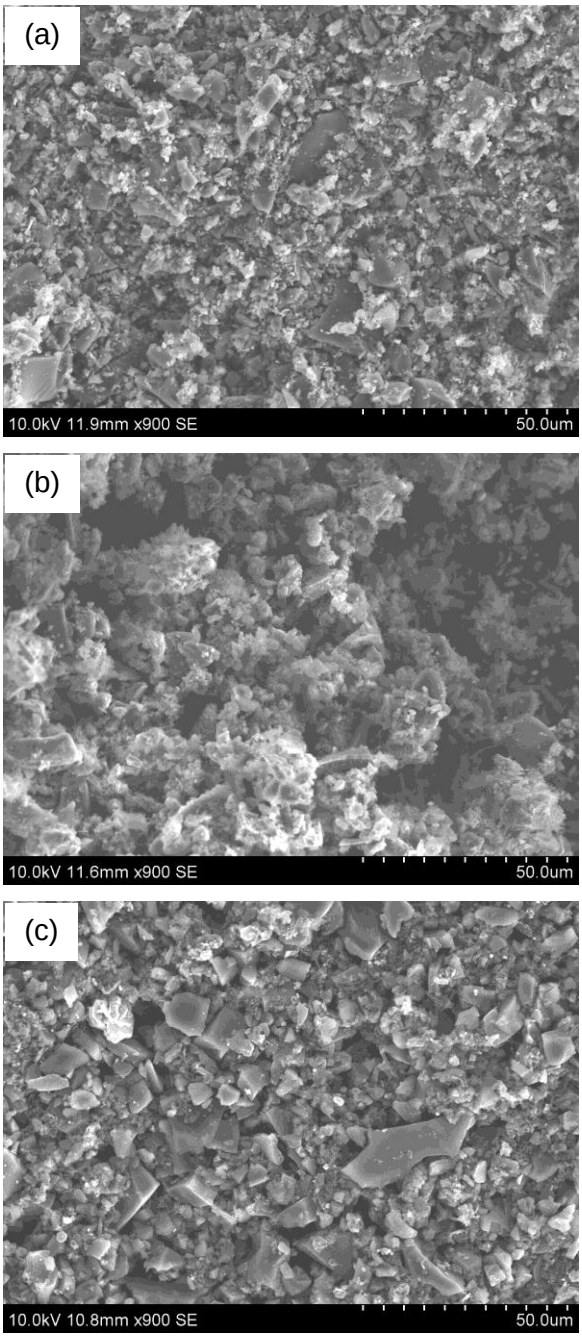

Fig. 2. SEM images of (a) untreated, (b) plasma activated, and (c) chemically activated biochar.

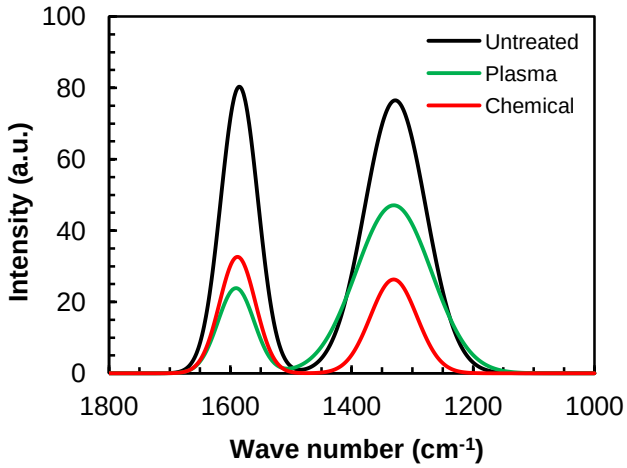

Fig. 3. Raman spectra of untreated, plasma activated, and chemically activated biochar.

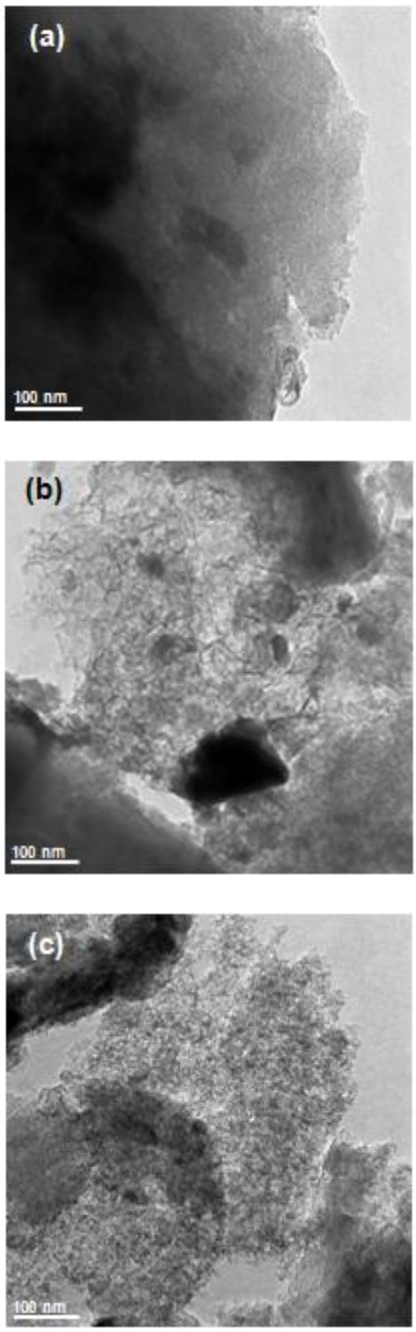

Fig. 4. TEM images of (a) untreated, (b) plasma activated, and (c) chemically activated biochar.

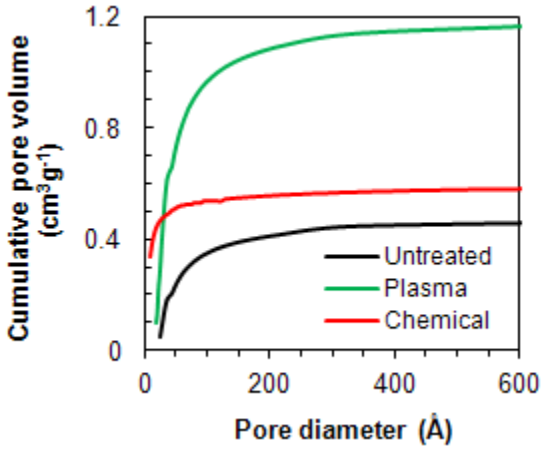

Fig. 5. Cumulative pore volume vs. pore diameter for untreated, plasma activated, and chemically activated biochar.

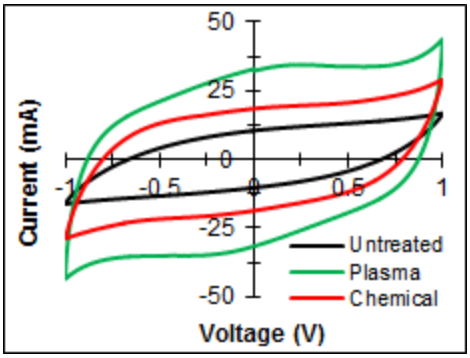

Fig. 6. CV curves of supercapacitors fabricated from untreated, oxygen plasma activated, and chemically activated biochar. The electrolyte was 6 mol/L KOH.

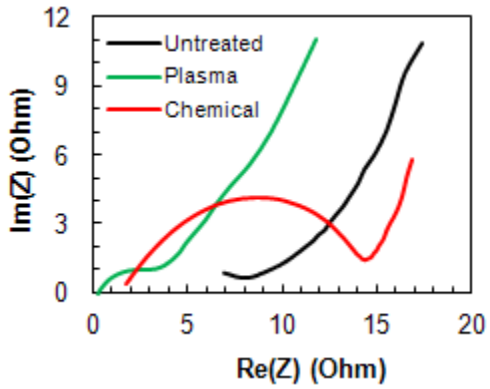

Fig. 7. EIS curves of untreated, oxygen plasma activated, and chemically activated biochar supercapacitors. The measurement frequency range was 0.1 to 10 KHz and voltage was 10 mV.

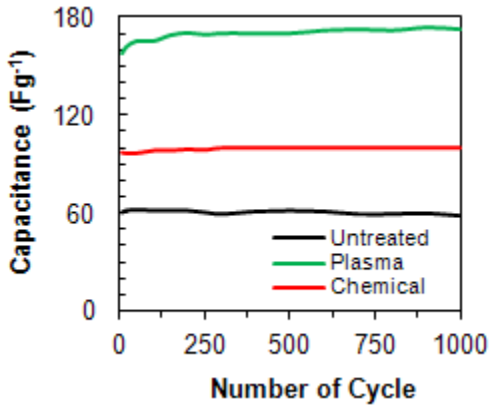

Fig. 8. Specific capacitance vs. number of charge/discharge cycles for untreated, oxygen plasma activated, and chemically activated biochar supercapacitors.

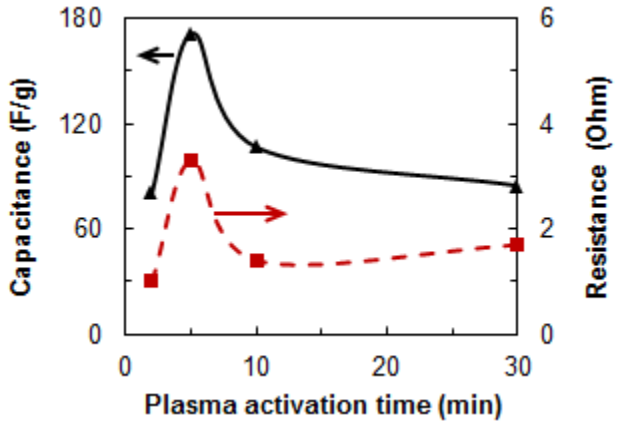

Fig. 9. Effects of plasma treatment time on the specific capacitance and resistance of the biochar supercapacitors.